



Einstein–Dirac–Maxwell wormholes: ansatz, construction and properties of symmetric solutions

Jose Luis Blázquez-Salcedo^{1,a} , Christian Knoll², E. Radu³

¹ Departamento de Física Teórica and IPARCOS, Universidad Complutense de Madrid, 28040 Madrid, Spain

² Institut für Physik, Universität Oldenburg, Postfach 2503, 26111 Oldenburg, Germany

³ Departamento de Matemática da Universidade de Aveiro and Centre for Research and Development in Mathematics and Applications (CIDMA), Campus de Santiago, 3810-183 Aveiro, Portugal

Received: 5 November 2021 / Accepted: 2 June 2022 / Published online: 15 June 2022
© The Author(s) 2022

Abstract We present a discussion of the traversable wormholes in Einstein–Dirac–Maxwell theory recently reported in e-Print: 2010.07317. This includes a detailed description of the ansatz and junction condition, together with an investigation of the domain of existence of the solutions. In this study, we assume symmetry under interchange of the two asymptotically flat regions of a wormhole. Possible issues and limitations of the approach are also discussed.

1 Introduction

The attempts to construct particle-like fermionic solutions have started with the work of Ivanenko [1], Weyl [2], Heisenberg [3] and Finkelstein et al. [4, 5], which considered a Dirac field model with a quartic self-interaction term. A rigorous numerical study of such solutions has been done by Soler in Ref. [6] (see also Ref. [7] for a proof of existence). The study of such localized configurations was mainly motivated as an attempt to construct models of extended particles.

In some sense, this type of solutions is the Dirac counterpart of the Q-balls [8] in a model with a complex self-interacting scalar field, sharing with them a variety of features [9]. Moreover, this analogy goes even further. As proven by Finster, Smoller and Yau [10] the inclusion of self-gravity effects leads to the existence of particle-like solitonic solutions of Einstein–Dirac equations even in the absence of a self-interaction term for the Dirac field (see also [11, 12] for early work in this direction). These Dirac solitons possess all basic properties of the mini-boson stars [13, 14], in particular some of the configurations being stable. Also, as with boson stars [15], no Black Hole (BH) horizon can be added at the center of a (spherically symmetric) Dirac soliton [16, 17].

Subsequent work includes extensions of the model in [10] with U(1) [18] or SU(2) [19] gauged fermions, or the study of Einstein–Dirac spinning configurations [20].

Note that in all aforementioned studies, the Dirac field was treated as a *quantum wave function*, its fermionic nature being imposed at the level of the occupation number: at most a single particle, in accordance to Pauli’s exclusion principle. Thus the second quantization effects are ignored, while the gravitational field is treated purely classically.

The Finster–Smoller–Yau solutions (together with their various generalizations) are topologically trivial, with a spacetime geometry which is a deformed Minkowski one. However, as found recently in Ref. [21], a Dirac field allows for another class of solutions which are absent in the usual models with bosonic fields – the traversable wormholes (WHs). In some sense, these solutions provide an explicit realization of Wheeler’s idea of “*electric charge without charge*” [22], possessing a variety of interesting properties.

The subject of traversable WHs has entered General Relativity (GR) with the work of Ellis [23] and Bronnikov [24], enjoying increasing interest over the last decades. A characteristic feature of a traversable WH is that it necessarily requires a matter content violating the null energy condition [25–27]. Then, restricting to a field theory source and a classical setting, the bosonic matter fields necessarily possess a non-standard Lagrangian (e.g. ‘phantom’ fields [23, 24, 28–30]). Another possibility is to consider extensions of gravity beyond GR (see e.g. [31, 32]).

The novelty of Ref. [21] was to show that the situation may change for fermions, with the existence of traversable WH solutions of the Einstein–Dirac(–Maxwell) equations. An *exact* WH solution with ungauged, massless fermions was also reported there, although with a spinor wave function which is not normalizable. The main purpose of this work is to provide a detailed description of the *numerical*

^a e-mail: jlblaz01@ucm.es (corresponding author)

solutions in Ref. [21] (which possess finite mass, charge and a normalizable spinor wave function), with emphasis on a number of technical details. The paper is organized as follows. The Sects. 2 and 3 deal with the general framework of the solutions. In particular, we discuss the issue of a symmetric Ansatz together with the junction condition at the WH throat. The numerical results are presented in Sect. 4. We end with Sect. 5, where the emerging picture is summarized. The Appendices contain details on the formalism used in the description of fermions in a curved geometry, together with a description of the numerical approach. An exact solution with ungauged, massless spinors is also discussed there.

2 The Einstein–Dirac–Maxwell action and field equations

We consider Einstein’s gravity minimally coupled with two U(1)-gauged relativistic fermions with equal mass, the spin of which is taken to be opposite in order to satisfy spherical symmetry. Working in units with $G = c = \hbar = 1$, the action of the corresponding Einstein–Dirac–Maxwell (EDM) model reads

$$S = \frac{1}{4\pi} \int d^4x \sqrt{-g} \left[\frac{1}{4}R + \mathcal{L}_D - \frac{1}{4}F^2 \right], \tag{2.1}$$

where R is the Ricci scalar of the metric $g_{\mu\nu}$, $F_{\mu\nu} = \partial_\mu A_\nu - \partial_\nu A_\mu$ is the field strength tensor of the U(1) field A_μ , and

$$\mathcal{L}_D = \sum_{\epsilon=1,2} \left[\frac{i}{2} \bar{\Psi}^{[\epsilon]} \gamma^\nu \hat{D}_\nu \Psi^{[\epsilon]} - \frac{i}{2} \hat{D}_\nu \bar{\Psi}^{[\epsilon]} \gamma^\nu \Psi^{[\epsilon]} - \mu \bar{\Psi}^{[\epsilon]} \Psi^{[\epsilon]} \right],$$

where μ is the mass of both spinors, q is the gauge coupling constant and $\hat{D}_\mu = \partial_\mu - \Gamma_\mu - iqA_\mu$.

Also, γ^ν are the curved space gamma matrices, while Γ_μ are the spinor connection matrices. Their expression is given in Appendix A, together with some other details on the spinor formalism, where we follow the notation and conventions in Ref. [33],

The resulting field equations are

$$R_{\mu\nu} - \frac{1}{2}Rg_{\mu\nu} = 2T_{\mu\nu} \text{ with } T_{\mu\nu} = T_{\mu\nu}^{(D)} + T_{\mu\nu}^{(M)}, \tag{2.2}$$

$$(\gamma^\nu \hat{D}_\nu - \mu)\Psi^{[\epsilon]} = 0, \quad \nabla_\mu F^{\mu\nu} = qj^\nu, \tag{2.3}$$

with the current

$$j^\nu = j^{\nu[1]} + j^{\nu[2]}, \text{ where } j^{\nu[\epsilon]} = \bar{\Psi}^{[\epsilon]} \gamma^\nu \Psi^{[\epsilon]}, \tag{2.4}$$

and the stress–energy tensor

$$T_{\mu\nu}^{(D)} = \sum_{\epsilon=1,2} T_{\mu\nu}^{(D)[\epsilon]} = -\frac{i}{4} \sum_{\epsilon=1,2} \left[\bar{\Psi}^{[\epsilon]} \gamma_\mu \hat{D}_\nu \Psi^{[\epsilon]} + \bar{\Psi}^{[\epsilon]} \gamma_\nu \hat{D}_\mu \Psi^{[\epsilon]} - \hat{D}_\nu \bar{\Psi}^{[\epsilon]} \gamma_\mu \Psi^{[\epsilon]} - \hat{D}_\mu \bar{\Psi}^{[\epsilon]} \gamma_\nu \Psi^{[\epsilon]} \right], \tag{2.5}$$

$$T_{\mu\nu}^{(M)} = F_{\mu\alpha} F_\nu^\alpha - \frac{1}{4}F^2 g_{\mu\nu}. \tag{2.6}$$

3 Spherically symmetric wormholes: the framework

3.1 The metric

Restricting to static, spherically-symmetric solutions of the field equations, we consider a general metric ansatz

$$ds^2 = g_{tt}(r)dt^2 + g_{rr}(r)dr^2 + g_{\Omega\Omega}(r)d\Omega^2 = -F_0^2(r)dt^2 + F_1^2(r)dr^2 + F_2^2(r)d\Omega^2, \tag{3.1}$$

where $d\Omega^2 = d\theta^2 + \sin^2\theta d\varphi^2$ is the line element on the two-sphere (θ and φ being spherical coordinates with the usual range), while r and t are the radial and time coordinates, respectively.

Particle-like (topologically trivial) solitons in EDM theory, are usually studied in Schwarzschild-like coordinates, with $0 \leq r < \infty$ and $F_2(r) = r$. However, the situation is more complicated for a WH geometry. The characteristic feature here is the existence of two asymptotically flat regions (the two sphere $r = const.$, $t = const.$ possessing a minimal, nonzero size), together with the absence of an event horizon.

A metric gauge choice which makes transparent the WH structure is

$$F_2(r) = \sqrt{r^2 + r_0^2}, \text{ with } -\infty < r < \infty, \tag{3.2}$$

where $r_0 > 0$ an input parameter—the radius of the throat.

Given the above ansatz, we choose the following vierbein (with $F_i > 0$):

$$e^r = \epsilon_r F_1 dr, \quad e^\theta = F_2 d\theta, \quad e^\varphi = F_2 \sin\theta d\varphi, \quad e^t = \epsilon_t F_0 dt, \tag{3.3}$$

where

$$\epsilon_r = \pm 1, \quad \epsilon_t = \pm 1. \tag{3.4}$$

The natural choice for particle-like configurations [10, 18], is $\epsilon_r = 1$. However, for a WH geometry, one takes instead

$$\epsilon_r = 1 \text{ for } r > 0 \text{ and } \epsilon_r = -1 \text{ for } r < 0, \tag{3.5}$$

a choice which takes into account the sign change of r at the WH’s throat [34].

3.2 The matter functions

In our work, we consider a purely electric Maxwell field with

$$A = V(r)dt, \tag{3.6}$$

$V(r)$ being the electrostatic potential.

The Ansatz for the Dirac fields is chosen such that (i) it allows for spherically symmetric geometries, and (ii) it leads to a stress tensor and field equations which are compatible with the ‘reflection’ symmetry $r \rightarrow -r$. A Dirac ansatz which satisfies these conditions can be written in terms of a single complex function z , with (see also Appendix B)

$$\Psi^{[1]} = \begin{pmatrix} z(r) \cos(\frac{\theta}{2}) \\ i\bar{z}(r) \sin(\frac{\theta}{2})\kappa \\ -i\bar{z}(r) \cos(\frac{\theta}{2}) \\ -z(r) \sin(\frac{\theta}{2})\kappa \end{pmatrix} e^{i(\frac{1}{2}\varphi - wt)},$$

$$\Psi^{[2]} = \begin{pmatrix} iz(r) \sin(\frac{\theta}{2}) \\ \bar{z}(r) \cos(\frac{\theta}{2})\kappa \\ \bar{z}(r) \sin(\frac{\theta}{2}) \\ iz(r) \cos(\frac{\theta}{2})\kappa \end{pmatrix} e^{i(-\frac{1}{2}\varphi - wt)}, \tag{3.7}$$

where $\kappa = \pm 1$ and w is the field frequency. Also, we note

$$z(r) = P(r) + iQ(r), \tag{3.8}$$

$P(r)$, $Q(r)$ being two real functions subject to some conditions discussed below. z can also be expressed in terms of an amplitude $|\phi_0|$ and a phase α ,

$$z(r) = |\phi_0|e^{i\alpha}, \text{ with } |\phi_0| = \sqrt{P^2 + Q^2}, \tan \alpha = \frac{Q}{P}. \tag{3.9}$$

3.3 The equations

Given the above ansatz, the Einstein equations read (where the prime denotes the derivative with respect to r):

$$\frac{F_0''}{F_0} + \frac{F_0'}{F_0} \left(\frac{F_2'}{F_2} - \frac{F_1'}{F_1} \right) - \frac{F_2'^2}{2F_2^2} + \frac{F_1'^2}{2F_2^2} - 2 \left(\frac{3V'^2}{4F_0^2} + 2F_1^2 (\epsilon_t(w + qV) \frac{(P^2 + Q^2)}{F_0} - \frac{\kappa(P^2 - Q^2)}{F_2}) \right) = 0,$$

$$\frac{F_2''}{F_2} + \frac{F_2'}{F_2} \left(\frac{F_2'}{2F_2} - \frac{F_1'}{F_1} \right) - \frac{F_1'^2}{2F_2^2} + \frac{1}{F_0} \left(\frac{V'^2}{2F_0} + 4\epsilon_t(w + qV)F_1^2(P^2 + Q^2) \right) = 0,$$

$$\frac{2F_0'F_2'}{F_0F_2} + \frac{F_2'^2 - F_1'^2}{F_2^2} + 2 \left(\frac{V'^2}{2F_0^2} + 4\epsilon_r F_1(PQ' - QP') \right) = 0. \tag{3.10}$$

The spinor functions P , Q satisfy the first order equations,

$$\epsilon_r P' + \epsilon_r \left(\frac{F_0'}{2F_0} + \frac{F_2'}{F_2} \right) P$$

$$+ \frac{F_1}{F_2} \left(\kappa - \frac{F_2}{F_0} \epsilon_t(w + qV) \right) Q - \mu F_1 P = 0,$$

$$\epsilon_r Q' + \epsilon_r \left(\frac{F_0'}{2F_0} + \frac{F_2'}{F_2} \right) Q + \frac{F_1}{F_2} \left(\kappa + \frac{F_2}{F_0} \epsilon_t(w + qV) \right) P + \mu F_1 Q = 0. \tag{3.11}$$

Finally, the Maxwell equations reduce to a second order equation for the electrostatic potential

$$\left(\frac{F_2^2 V'}{F_0 F_1} \right)' = 4\epsilon_t q F_1 F_2^2 (P^2 + Q^2). \tag{3.12}$$

Note that above equations are left invariant by the transformation

$$w \rightarrow w - \beta, \quad V \rightarrow V + \beta/q, \tag{3.13}$$

with β an arbitrary constant.

3.4 The ‘reflection’ symmetry and the junction condition

Here we discuss the junction conditions for the solutions with ‘reflection’ symmetry. The WH consists in two different regions Σ_{\pm} . The ‘up’ region (Σ_+) is found for $0 < r < \infty$, while the ‘down’ region (Σ_-) has $-\infty < r < 0$. These regions are joined at $r = 0$, which is the position of the throat.

In this work, we are interested in geometries which are invariant under a reflexion with respect to the throat, $r \rightarrow -r$. Therefore the metric functions and the energy-momentum tensor satisfy the conditions

$$F_i(-r) = F_i(r), \quad (i = 0, 1, 2) \text{ and } T_{\mu}^{\nu}(r) = T_{\mu}^{\nu}(-r). \tag{3.14}$$

As for the spinor functions, we impose the following condition

$$P(-r) = P(r), \quad Q(-r) = Q(r). \tag{3.15}$$

With these assumptions, it is straightforward to verify that the equations (3.10)–(3.12) remain invariant under the transformation $r \rightarrow -r$, taken together with (3.5) and (3.15). Here, we also assume that the product $\epsilon_t(w + qV)$ does not change sign. With respect to this, one distinguishes two possibilities. The first one is to take

$$(i) \quad \epsilon_t = 1 \text{ and } w \rightarrow w, \quad V \rightarrow V \text{ as } r \rightarrow -r. \tag{3.16}$$

The second choice is rather unusual, employing a *time reversed* frame in the Σ_- -region, *i.e.* with $t \rightarrow -t$ and

$$(ii) \quad \epsilon_t \rightarrow -\epsilon_t \text{ and } w \rightarrow -w, \quad V \rightarrow -V \text{ as } r \rightarrow -r, \tag{3.17}$$

(with the usual choice $\epsilon_t = 1$ for $r > 0$). Note that the product wt (which enter the spinor phase), as well as the one form $A = V(r)dt$ are invariant for both choices above.

However, the distinction between the possibilities (i) and (ii) above does not manifest at level of the construction of solutions, together with their basic properties. Also, let us remark that the identification (3.15) does not lead to a discontinuity of the amplitude or the phase of the spinor function z at the throat, $r = 0$.

Turning now to the joining at $r = 0$ of the line elements for Σ_{\pm} regions, one remarks that in general this is not ‘smooth’, with a discontinuity of the metric derivatives. This implies the presence of a thin mass shell structure at the throat, with a δ -source (*i.e.* a thin matter shell) added to the action (2.1). To get insight into this aspect, we evaluate the second fundamental form

$$K_{\mu\nu} = \frac{1}{2}(\nabla_{\mu}n_{\nu} + \nabla_{\nu}n_{\mu}) \quad (3.18)$$

at $r = 0^{\pm}$, with n_{ν} the unit vector normal at the surface $r = 0$. A straightforward computation shows that, at the throat, the only nonvanishing component of $K_{\mu\nu}$ is

$$K_{tt}|_{r=0^{\pm}} = \frac{F_0 F_0'}{F_1} \Big|_{r=0^{\pm}}. \quad (3.19)$$

However, for all solutions reported in this work, the first derivative of the metric function F_0 vanishes at $r = 0$. As such, $K_{\mu\nu} = 0$, meaning that the total stress–energy tensor of the configurations is free of surface energy densities, and no extra-matter distribution at the throat is required from this direction.

Let us comment here that solutions constructed via possibility (i) posses a feature that is potentially undesirable: the derivative of the gauge field is discontinuous at the throat (unless it vanishes, which interestingly as we will show later, is never the case in our construction). Such jump in the derivative involves a surface charge distribution, as observed in [35]. However this jump does not enter the total stress–energy tensor, and in fact, since the solutions satisfy $K_{\mu\nu} = 0$, the wormholes are free of surface energy densities at the throat.

Nonetheless, the discontinuity in the derivative of the gauge field can be avoided by implementing a matching under possibility (ii). The choice of a *time reversed* frame in the Σ_{-} -region obviously results in the absence of discontinuities in the gauge field derivatives, and hence no surface deltas appear in this case.

As noted in [35], the *time reversed* frame is in fact equivalent to a change in the sign of the gauge coupling constant. This means that solutions with charge q in the Σ_{+} region are matched to solutions with $(-q)$ in the Σ_{-} region. This is related with the ‘classical’ interpretation of a time reversed Dirac field, *i.e.* if a wave function describes the state of a particle, the time-reversed wave function describes the state

of an *antiparticle*. In light of this, the wormholes that we discuss in the paper can be interpreted as being supported by a Dirac matter field in the Σ_{+} region, and the corresponding antimatter in the Σ_{-} region.

Finally, let us note here that the choice of spinor in region Σ_{-} given by Eq. (3.15) is not the only possibility. Similar results are found when considering instead a different Dirac-ansatz for the ‘down’-region (still in terms of two real functions (P, Q)), together with a different identification instead of (3.15) [21]. However, the picture becomes more complicated in this case, with a discontinuity of the spinors’ phase at the throat [21,35]. Although the discontinuity in the phase does not translate into surface energy densities at the level of the total stress–energy tensor, this matching may not be completely desirable from a physical point of view, as it results in surface deltas in the Dirac field equation at the throat. Nonetheless, it is interesting to note that for this construction, the ‘up and ‘down’ spinors can be related at the junction via an unitary transformation, with a similar construction having been discussed before in [34].

3.5 Asymptotics and boundary conditions

For $r \rightarrow \pm\infty$, the Minkowski spacetime geometry is approached, the spinor functions vanish, while the electric potential approached a constant value

$$F_0|_{r=\pm\infty} = F_1|_{r=\pm\infty} = 1, \quad P|_{r=\pm\infty} = Q|_{r=\pm\infty} = 0, \quad V|_{r=\pm\infty} = \epsilon_t \Phi. \quad (3.20)$$

At the throat, one imposes

$$F_0|_{r=0^{\pm}} = F_{00}, \quad F_1|_{r=0^{\pm}} = F_{10}, \quad V|_{r=0^{\pm}} = 0, \quad (3.21)$$

(note that the condition for a vanishing electric potential fixes the residual gauge freedom (3.13)), while

$$P|_{r=0^{\pm}} = p_0, \quad Q|_{r=0^{\pm}} = q_0, \quad (3.22)$$

with $F_{00} > 0$, $F_{10} > 0$, and p_0, q_0 arbitrary constants. To simplify the picture, we have restricted our numerical study to solutions with $p_0 = -q_0$.

The solutions interpolating between the above asymptotics are found numerically, as described below. However, one can construct an approximate local solution compatible with the above condition. For example, the first terms in a large- r expression are

$$F_0 \rightarrow 1 - \frac{M}{r} + \dots, \quad F_1 \rightarrow 1 + \frac{M}{r} + \dots, \quad V \rightarrow \Phi - \frac{Q_e}{r}, \quad P \rightarrow \frac{p_{\infty}}{r} e^{-\mu_* r} + \dots, \quad Q \rightarrow \frac{q_{\infty}}{r} e^{-\mu_* r} + \dots, \quad (3.23)$$

with M and Q_e the mass and electric charge. Also, $p_{\infty} = -c_{\infty}(\frac{\mu_*}{\mu - w_*} - 1)$, $q_{\infty} = c_{\infty}(\frac{\mu_*}{\mu - w_*} + 1)$ (with c_{∞} a constant

and $w_* = w + q\Phi$). In the above relations we note $\mu_* = \sqrt{\mu^2 - w_*^2}$, with the bound state condition $\mu^2 > w_*^2$.

A local solution can also be constructed close to the throat, as a power series in r . For example, the metric functions behave as¹

$$\begin{aligned} F_0(r) &= F_{00} + F_{02}r^2 + \dots, \\ F_1(r) &= F_{10} + \epsilon_r F_{11}r + F_{12}r^2 + \dots, \end{aligned} \tag{3.25}$$

where F_{02}, F_{12} are complicated expressions in terms of the input parameters and the values at $r = 0$ of various functions, while F_{11} is a undetermined constant. Note that a value $F_{11} \neq 0$ implies discontinuity at the throat for the first derivative of metric function g_{rr} . A systematic investigation of all numerical solutions constructed so far reveals that all of them have $F_{11} \neq 0$. Therefore this feature seems to be generic, provided that the solutions are required to be symmetric around the throat.² On the other hand, solutions with $F'_1(0) = 0$ and $F'_0(0) = 0$ appear to exist in a model with asymmetric wormholes [36] (suggested also in [37]).

As for the electrostatic potential, all solutions studied so far have a nonzero electric field at the throat, $V'(0) \neq 0$. For the (usual) choice (3.16) with $\epsilon_t = 1$ and $V(r) = V(-r)$, this implies that the electric field is discontinuous at $r = 0$, with

$$V(r) = \epsilon_r v_1 r + \dots, \text{ and } F_{rt}|_{r=0^+} = -F_{rt}|_{r=0^-} = v_1. \tag{3.27}$$

The jump in the electric field at the throat implies the presence of a thin shell of electric charge located at $r = 0$. That is, for consistency, the action (2.1) should be supplemented with a

¹ The leading order terms which enter the near-throat expansion satisfy the constraints (with $v_1 = V'(0^+)$):

$$\begin{aligned} \frac{1}{r_0^2} &= 8q_0^2 F_{10}^2 (\mu - \frac{2w}{F_{00}}), \quad 8q_0^2 \left(\mu + (1 - F_{10}^2)(\mu - \frac{2w}{F_{00}}) \right) \\ &+ \frac{v_1^2}{F_{00}^2 F_{10}^2} = 0. \end{aligned} \tag{3.24}$$

² Note that the constant F_{11} does not enter the expression of the Riemann tensor evaluated at the throat. As for curvature invariants, one finds

$$\begin{aligned} R|_{r=0^\pm} &= \frac{2}{r_0^2} \left(1 - \frac{2}{F_{10}^2} - \frac{2F_{02}r_0^2}{F_{00}F_{10}^2} \right), \quad K|_{r=0^\pm} \\ &= \frac{4}{r_0^4} \left(1 + \frac{2}{F_{10}^4} \right) + \frac{16F_{02}^2}{F_{00}^2 F_{10}^4}, \end{aligned} \tag{3.26}$$

for the Ricci and Kretschmann scalars, respectively. Moreover, when expressing the line-element in terms of the normal coordinate to the throat $\eta = \int F_1 dr$ (with $g_{\eta\eta} = 1$ and the following expression for small $|r|$: $\eta = F_{10}r + \epsilon_r F_{11}r^2/2 + \dots$), one finds the first derivatives of both $g_{tt}(\eta)$ and $g_{\Omega\Omega}(\eta)$ vanish at the throat.

term

$$S_\Sigma = \frac{1}{4\pi} \int d^4x \sqrt{-g} A_\nu J^\nu, \quad \text{with } J^\nu = \sigma_0 u^\nu \delta(r) \tag{3.28}$$

and the unit vector $u^\nu = \delta_t^\nu / F_0$. Also, σ_0 is the throat charge density,

$$\sigma_0 = \frac{2v_1}{F_1^2 F_0}, \tag{3.29}$$

as resulting from a straightforward computation. The ($r = 0$ localized) stress–energy tensor associated with this charge distribution is

$$T_{\alpha\beta}^{(s)} = A_\alpha \tilde{J}_\beta + A_\beta \tilde{J}_\alpha - h_{\alpha\beta} A_\nu \tilde{J}^\nu, \tag{3.30}$$

where $h_{\alpha\beta}$ denotes the three-dimensional induced metric on the throat and $\tilde{J}^\nu = \sigma u^\nu$. Since the U(1)-potential is vanishing at the throat, $T_{\alpha\beta}^{(s)}$ does not contribute to the Einstein equations evaluated at $r = 0$.

A different picture is found for the choice (3.17) of the mapping between Σ_\pm -regions, with $V(-r) = -V(r)$ and the near-throat expression $V(r) = v_1 r + O(r^2)$. As a result, $F_{rt}|_{r=0^+} = F_{rt}|_{r=0^-}$, in which case no extra-matter exists at the WH throat.

3.6 Quantities of interest and a Smarr law

The only global charges of the solutions are the mass M and the electric charge Q_e . The WHs also possess a nonzero throat area

$$A_t = 4\pi r_0^2. \tag{3.31}$$

Also, for each spinor, one defines a Noether charge Q_N . Restricting to the Σ_+ -region, the expression of Q_N reads

$$\begin{aligned} Q_N^{[1]} &= Q_N^{[2]} = Q_N = \frac{1}{4\pi} \int_{\Sigma_+} d^3x \sqrt{-g} j^{t[\epsilon]} \\ &= 2 \int_0^\infty dr F_1 F_2^2 (P^2 + Q^2). \end{aligned} \tag{3.32}$$

Because we are restricting to symmetric solutions with respect reflection around the throat, the Noether charge Q_N is the same in the Σ_- -region

$$\begin{aligned} Q_N &= \frac{1}{4\pi} \int_{\Sigma_-} d^3x \sqrt{-g} j^{t[\epsilon]} \\ &= 2 \int_0^{-\infty} dr F_1 F_2^2 (P^2 + Q^2). \end{aligned} \tag{3.33}$$

By integrating the Maxwell equations, one finds

$$Q_e = 2q Q_N + Q_T, \tag{3.34}$$

with $Q_T = V'(0^+)r_0^2 / (F_0(0)F_1(0))$.

The WHs satisfy a Smarr law, the mass being the sum of an electrostatic term and a bulk contribution

$$M = \Phi Q_e + M_{(B)}, \quad (3.35)$$

with

$$M_{(B)} = 4 \int_0^\infty dr F_1 F_2^2 [2\mu F_0 P Q + (2w + qV)(P^2 + Q^2)].$$

Similar relations hold for the Σ_- -region, in agreement with the reflection symmetry of the solutions.

Wormholes are well known to violate the null energy condition (NEC) [25–27, 32], and we will show that the ones that we construct in this paper are no exception. NEC requires the total stress–energy tensor of the system to satisfy the following relation $T_{\mu\nu} v^\mu v^\nu > 0$, where v is any null vector, $v^2 = 0$. In our case, NEC can be further simplified into the following expression,

$$T_r^r - T_t^t = \frac{1}{F_1} (Q P' - P Q') - \epsilon_t \frac{P^2 + Q^2}{F_0} (qV + \omega) > 0. \quad (3.36)$$

This is clearly not a positive definite expression, and we will see later that the solutions we construct in this paper violate this condition at every point.

3.7 Scaling symmetry and one particle condition

The equations of the model are invariant under the scaling transformation (the variables and quantities which are not specified remain invariant):

$$\begin{aligned} (r, r_0) &\rightarrow \lambda(r, r_0), & (P, Q) &\rightarrow (P, Q)/\sqrt{\lambda}, \\ (\mu, q, w) &\rightarrow (\mu, q, w)/\lambda, \end{aligned} \quad (3.37)$$

where λ is a positive constant, while various quantities of interest transform as

$$(M, Q_e) \rightarrow \lambda(M, Q_e), \quad (Q_N, A_t) \rightarrow \lambda^2(Q_N, A_t). \quad (3.38)$$

As with the Einstein–Dirac(–Maxwell) solitons [10, 18, 38], this transformation is used to impose the one particle condition, $Q_N = 1$, for *each* spinor in both ‘up’ or ‘down’ regions. That is, solving numerically the field equations with some input values of $\{\mu, q, r_0, w\}$ one finds a solution with a nonzero $Q_N^{(num)}$. Then the physical solution with $Q_N = 1$ results from (3.37), (3.38), with $\lambda = 1/\sqrt{Q_N^{(num)}}$.

Let us also remark that only quantities which are invariant under the transformation (3.37), (3.38) (like M/Q_e or A_t/Q_e^2) are relevant.

4 Numerical solutions

In this section we analyze the properties of the symmetric and smooth WHs that are obtained within the setting described in

the previous sections. In order to obtain the WH solutions, we solve numerically the field equations, imposing the boundary conditions that follow from the expansions at infinity and around the throat. More details on the specific parametrization, the equations that are solved in practice and numerical solver are provided in Appendix C.

As mentioned above, all solutions discussed here are symmetric with respect to a reflection at the throat, and satisfy the condition $F'_0(0) = 0$, while $F'_1(0^+) = -F'_1(0^-) \neq 0$. Also, to simplify the picture, we shall restrict our study to fundamental solutions (*i.e.* no radial excitations of the spinors) and, moreover, we shall display the profiles of various functions of interest for $r \geq 0$ only.

4.1 Solutions’ properties

Let us start by describing the generic features of the metric and matter functions that characterize these WHs.

In Fig. 1 we show the typical profile for the metric functions g_{tt} (left) and g_{rr} (right), versus the compactified coordinate ρ (as defined by the Eq. (C.1) in Appendix C), with

$$r^2 + r_0^2 = \frac{r_0^2}{(1 - \rho^2)^2}. \quad (4.1)$$

For these solutions we fix the parameters of the theory to $q = 0.1$ and $\mu = 0.5$. Then WHs can be obtained for fixed values of the electric charge $Q_e = 4.55$ and $\kappa = 1$, with different values of the parameter $w_* = w + q\Phi$. These are $w_* = \{-\mu, -0.4, 0, 0.08\}$, being shown in Fig. 1 in red, purple, blue and orange respectively. As a comparison we also include the corresponding metric functions for the extremal RN (eRN) BH (dashed black curves). As we can see in the figure, for $w_* = 0.08$, the metric functions overlap those of extremal RN, differing only close to the throat. The numerical results suggest that in the limit $w_* \rightarrow q$, the metric functions tend to become closer and closer to the extremal RN functions.³ In the limit, the throat develops a degenerate event horizon, and the solution coincides with extremal RN. No smooth solutions can be found for $w_* > q$. Hence we conclude that extremal RN forms one of the boundaries of the domain of existence of the WHs.

The solutions with $w_* = -\mu$ form the other boundary of the configuration space (red curve). We will refer to these WHs as ‘limit’ solutions, since the domain of existence cannot be extended beyond this value of the frequency. We find that this is a generic feature, also valid for other arbitrary values of the parameters: all the smooth and symmetric WH solutions we have obtained exist only for $-\mu \leq w_* < q$. In many cases, like in the example shown in Fig. 1, these limit configurations possess negative masses, and we will see that this depends on the particular values of q/μ .

³ In the numerics, this limit is approached as $w \rightarrow 0$ and $\Phi \rightarrow 1$.

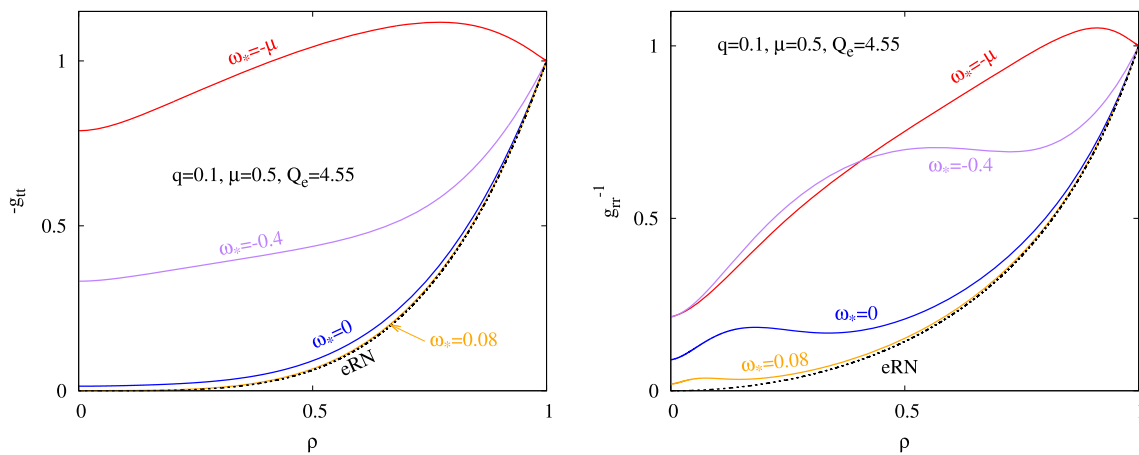


Fig. 1 Metric functions g_{tt} (left) and g_{rr} (right), versus the compactified coordinate ρ . Each color corresponds to a solution with $w_* = \{-\mu, -0.4, 0, 0.08\}$ (red, purple, blue and orange respectively),

The extremal RN function is shown for comparison with a black dashed curve. All solutions have $q = 0.1, \mu = 0.5, Q_e = 4.55, \kappa = 1$. Also, in all plots we define $w_* = w + q\Phi$

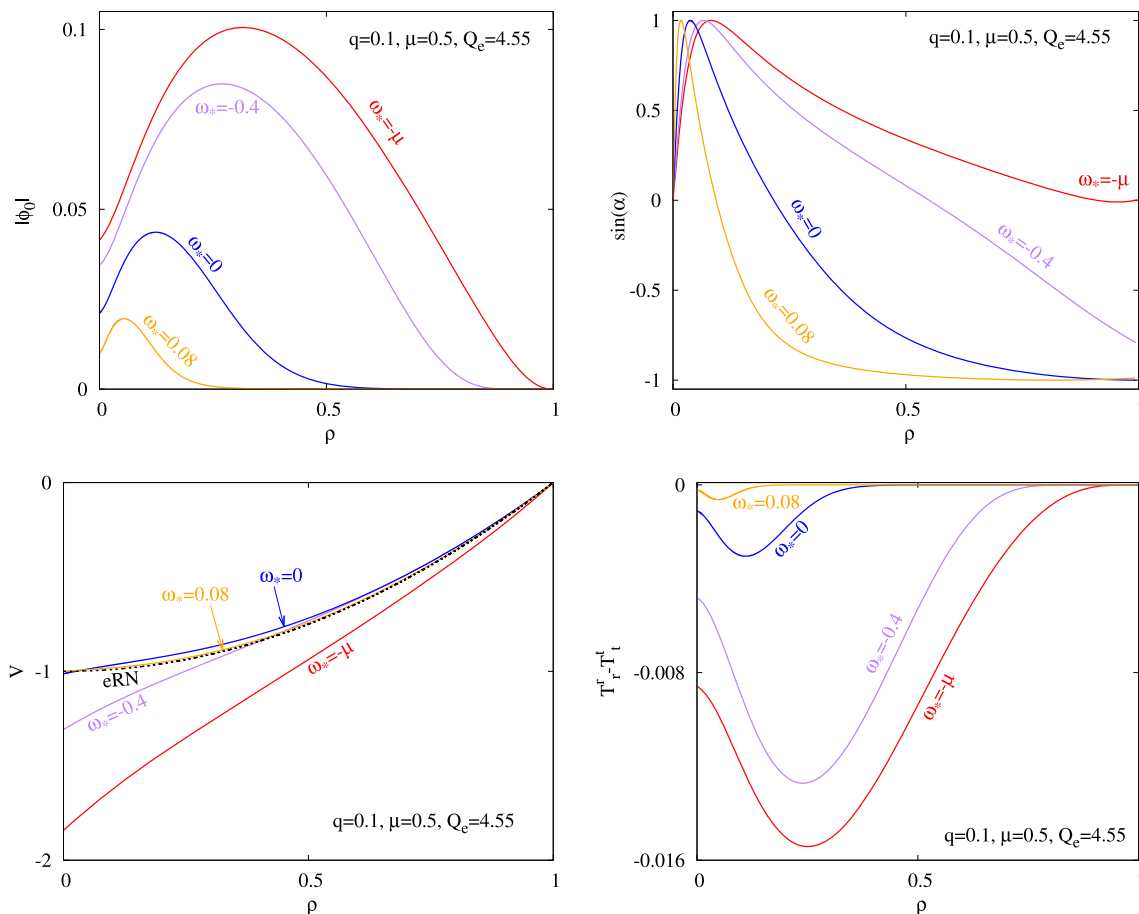


Fig. 2 Matter functions $|\phi_0|$ (top left), $\sin(\alpha)$ (top right), V (bottom left) and $T_r^r - T_t^t$ (bottom right) versus the compactified coordinate ρ . Each color corresponds to a solution with $w_* = \{-\mu, -0.4, 0, 0.08\}$ (red, purple, blue and orange respectively). All solutions have $q = 0.1, \mu = 0.5, Q_e = 4.55, \kappa = 1$

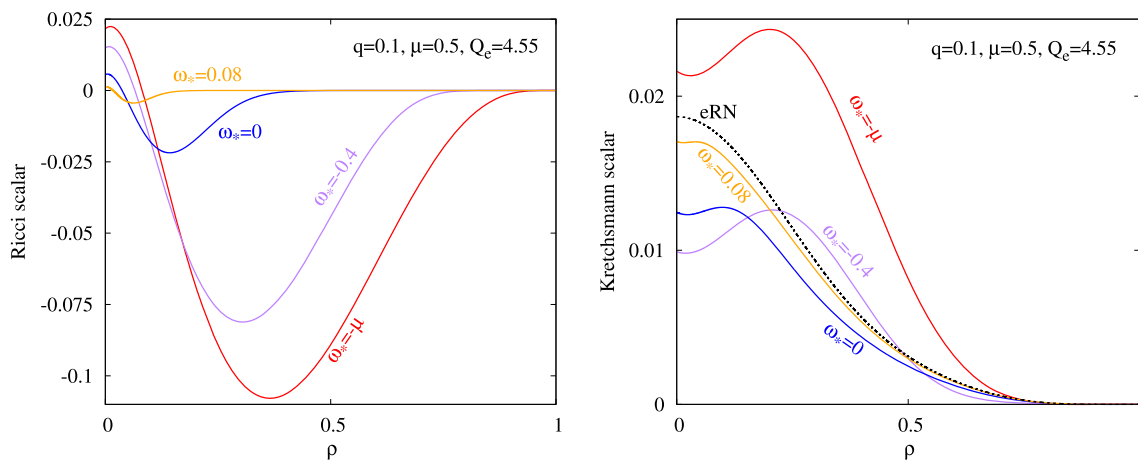


Fig. 3 Ricci scalar (left) and Kretschmann scalar (right) as a function of the compactified coordinate ρ . Each color corresponds to a solution with $w_* = \{-\mu, -0.4, 0, 0.08\}$ (red, purple, blue and orange respectively). All solutions have $q = 0.1$, $\mu = 0.5$, $Q_e = 4.55$, $\kappa = 1$

Next we discuss the behaviour of the matter content. As an example, in Fig. 2 we show the profiles of the matter functions, for the same value of the parameters as in the previous figure.

The amplitude of the Dirac field ϕ_0 is shown in Fig. 2 (top left). For all solutions the Dirac field decays exponentially as approaching the asymptotic boundaries. The Dirac field of the 'limit' solutions also decays exponentially at the boundaries (but with a slightly weaker exponential decay, since $\mu_* = 0$), meaning that these solutions represent also localized states. Hence all the smooth WHs with $-\mu \leq w_* < q$ correspond to localized states that can be consistently rescaled to $Q_N = 1$ (note that the profiles shown in this section are not rescaled). As w_* is increased towards $w_* = q$, the amplitude of the Dirac field decreases as it shrinks around the throat.

The other function that characterizes the Dirac spinors is the phase function α , which is shown in Fig. 2 (top right). The phase varies smoothly as we move away from the throat, and the difference in values between the throat and infinity depends on the value of w_* .

All the smooth configurations we have obtained are necessarily electrically charged, and hence they possess a non-trivial electric potential. We show the electric field function V in Fig. 2 (bottom left), where we fix the gauge so that the electric field is zero at $\rho = 1$. Again we note that the electric field becomes closer and closer to extremal RN as we increase $w_* \rightarrow q$, while it differs the most for the 'limit' configuration.

Another function of interest in order to characterize the matter content of these solutions is $T_r^r - T_t^t$, which is obtained from the respective components of the stress–energy tensor and characterizes the NEC, see Eq. (3.36). When this function is negative, the null energy condition is violated. We show this function in Fig. 2 (bottom right) versus the compactified

coordinate ρ where we can see that the null energy condition is violated everywhere. A comparison with the amplitude ϕ_0 reveals that the violation is maximal close to where the spinor amplitude is larger, which in fact happens slightly outside of the throat.

Let us now consider the curvature invariants for the same configurations we have been discussing. In Fig. 3 (left) we show the Ricci scalar, and in Fig. 3 (right) the Kretschmann scalar. One can see that these curvature invariants are everywhere regular for all the configurations with $-\mu \leq w_* < q$.

Finally, let us remark that the properties of the profiles described in this Section were found to be generic for other values of the theory parameters (q , μ), electric charge (Q_e) and κ . In particular, both the Ricci and Kretschmann scalars are *finite* and *smooth* functions everywhere, in particular at the throat, $r = 0$.

4.2 Domain of existence and global properties

From the previous profiles, we can extract all the global quantities that characterize the WHs: total charge, mass, throat area, Q_N , etc. All the solutions we consider can be appropriately rescaled so that $Q_N = 1$. However, for the study of the domain of existence it is convenient to consider appropriate adimensional products of the global quantities.

In the following we explore the properties of solutions with fixed values of the ratio q/μ . It is then possible to generate families of WHs with fixed values of the adimensional electric charge μQ_e . Solutions with fixed values of q/μ and μQ_e form a 1-parameter family of WHs, that extend from the limit configuration with $w_*/\mu = -1$ to the extremal RN BH with $w_*/q = 1$.

In order to compare the global quantities of these WHs with the extremal RN BH, it is useful to consider global quantities scaled to the electric charge of the configuration.

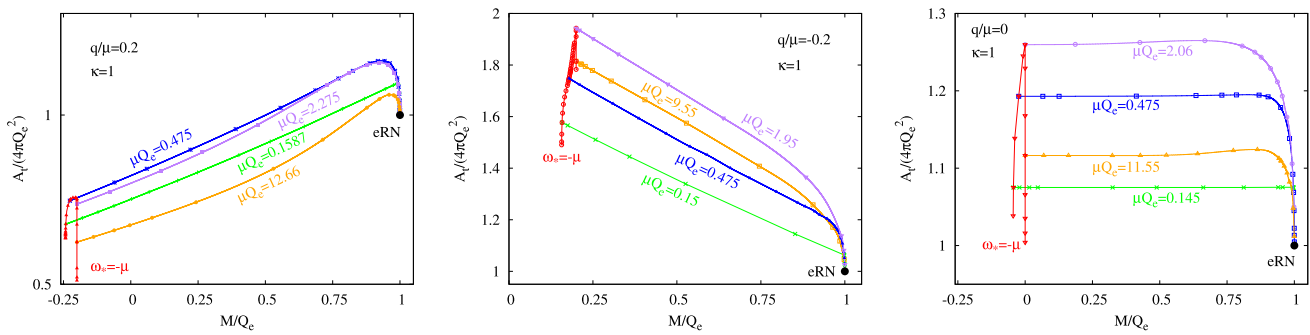


Fig. 4 Throat area scaled to the electric charge, $A_t/(4\pi Q_e^2)$, as a function of the scaled total mass, M/Q_e . Top left panel shows solutions for $q/\mu = 0.2$, top right panel for $q/\mu = -0.2$, and bottom panel for $q/\mu = 0$. Solutions with fixed scaled electric charge μQ_e are shown in

different colors (orange, purple, blue, green). Limit configurations with $w_* = -\mu$ are shown in red. The black dot represents the extremal RN BH. All these WHs are found for $\kappa = 1$

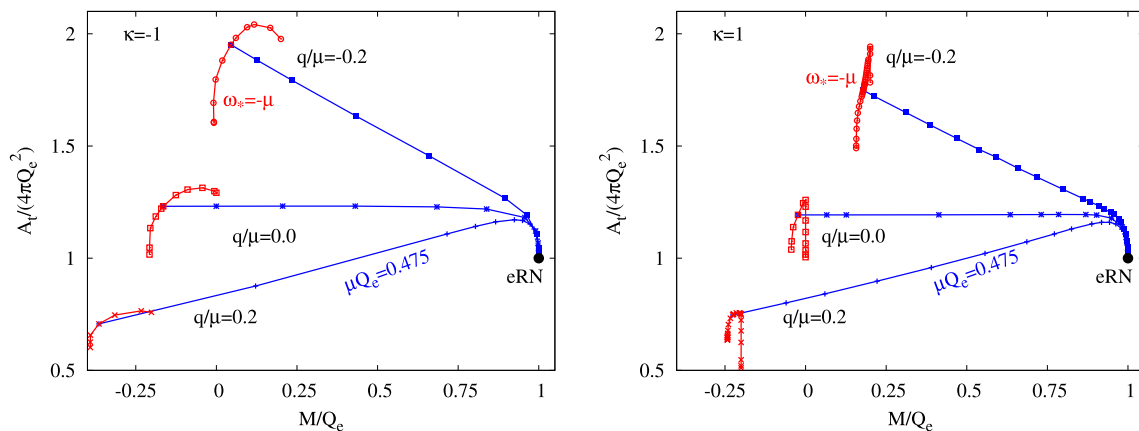


Fig. 5 Throat area scaled to the electric charge, $A_t/(4\pi Q_e^2)$, as a function of the scaled total mass, M/Q_e , for $\kappa = -1$ (left) and $\kappa = 1$ (right). Limit configurations with $w_* = -\mu$ are shown in red, while the blue curves represent solutions with fixed $\mu Q_e = 0.475$. The black dot indicates the extremal RN BH

In Fig. 4 we show the scaled throat area, $A_t/(4\pi Q_e^2)$, as a function of the scaled total mass, M/Q_e . Top left figure is for $q/\mu = 0.2$, top right figure is for $q/\mu = -0.2$, and bottom figure for $q/\mu = 0$. Each color curve corresponds to a family of solutions with different values of μQ_e . The red curve corresponds to the limit configurations with $w_* = -\mu$. The black dot indicates the extremal RN BH, for which the scaled horizon area and mass are equal to one. All these solutions have $\kappa = 1$.

Branches of solutions with constant μQ_e extend in between extremal RN (black dot) and the set of limit solutions (red curve). The ratio M/Q_e is maximal at the extremal RN solution ($M/Q_e = 1$), while the smallest mass possible is found for configurations on the limit curve. Depending on the theory, i.e. the value of q/μ , these limit masses can take negative values. Note that for $q/\mu = 0.2$ (top right), all the limit configurations have relatively large negative masses. In fact, for large values of μQ_e , the solutions on the limit curve tend to $M/Q_e = -q/\mu$. The solutions form a vertical

line where the area decreases with increasing μQ_e , while the mass-charge ratio is essentially fixed to $-q/\mu$.

Regarding the area, in Fig. 4 we can see that solutions sufficiently close to extremal RN possess throat areas larger than the corresponding horizon area of the extremal RN BH. In fact this happens for all mass-charge ratios in models with $q/\mu \leq 0$. Only in models with $q/\mu > 0$, it is possible to obtain configurations that possess throat areas smaller than the extremal RN horizon area.

While in Fig. 4 we have fixed $\kappa = 1$, the properties of solutions with $\kappa = -1$ do not differ significantly. In Fig. 5 we show again the scaled throat area as a function of the scaled mass. In Fig. 5(left) we show some subsets of solutions with $\kappa = -1$, and in Fig. 5(right) we show similar subsets with $\kappa = 1$. Qualitatively, the domain of existence is very similar for both values of κ , the most important differences appearing only close to the limit configurations.

Finally, let us comment that we have not found regular symmetric solutions for models with $|q/\mu| > 1$, nor WHs with $|M/Q_e| > 1$. Such configurations may exist in a more

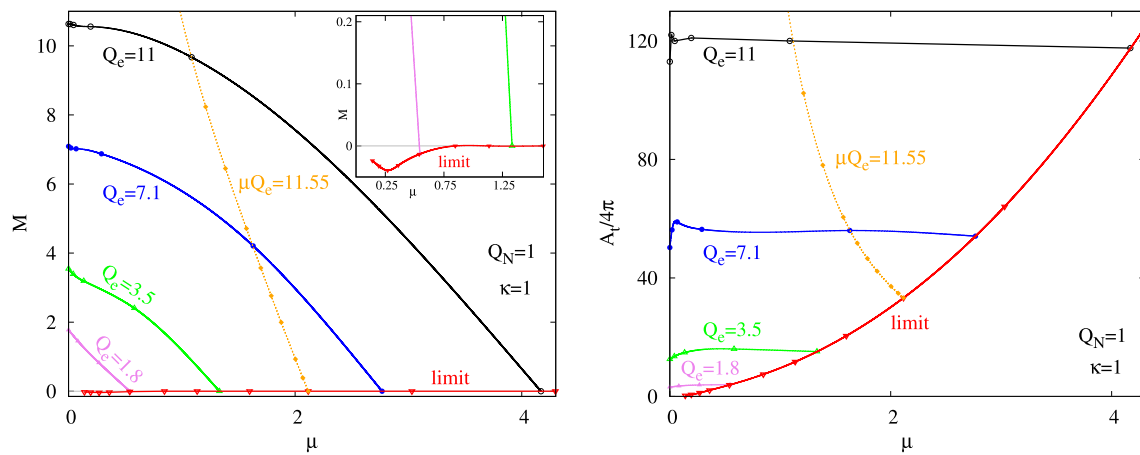


Fig. 6 (left) Mass M vs μ in Plank units for solutions with $q = 0$. The color curves correspond to families of solutions with fixed electric charge ($Q_e = 1.8, 3.5, 7.1, 11$ in pink, green, blue and black respectively). In red we show the limit configurations with $w_* = -\mu$. In

orange we include the solutions with fixed $\mu Q_e = 11.55$ for comparison with Fig. 4. (right) Same figure for the throat area A_t as a function of μ

general setting, for instance when considering asymmetric WHs.

4.3 Isocharge ensembles

The previous analysis in terms of adimensional quantities is useful in order to understand the domain of existence of these WHs. It also allows us to compare the properties of the WHs relative to the ones of the extremal RN BH, which plays a key role as it is one boundary of the space of solutions.

In order to make contact with previous analysis of Finster-Smoller-Yau solitons, in the following we will discuss the properties of the WHs in terms of the Plank scale. To do so we rescale all quantities to $Q_N = 1$, and look at ensembles of solutions with fixed values of the electric charge Q_e . These ensembles form again a 1-parameter family of solutions, characterized by the spinor mass μ .

In Fig. 6(left) we show the mass of the WH as a function of the mass of the fermion. For simplicity here we focus on the ungauged case with $q = 0$. The solid color curves represent the ensembles of fixed electric charge ($Q_e = 1.8, 3.5, 7.1, 11$ in pink, green, blue and black respectively). The red curve corresponds to the limit set, for which $w_* = -\mu$. Along this curve, the electric charge increases with the fermion mass. For reference, we also include the dotted orange curve, representing the family of configurations with fixed $\mu Q_e = 11.55$ that is shown in Fig. 4(bottom).

The WH solutions bifurcate from $\mu = 0$, for which we have seen that there is no fermion content, the configuration corresponding to the extremal RN BH with $M = Q$. Along the isocharge ensembles, the mass of the WH decreases monotonically with increasing fermion mass. Eventually, a limit value of μ is reached, for which $w_* = -\mu$ (limit red

curve). These solutions possess negative values of the mass, as shown in the inset figure.

Another quantity of interest is the throat area. In Fig. 6(right) we show the area as a function of the fermion mass in Plank units, for the same sets of solutions as for Fig. 6(left). We can see that for the isocharge ensembles, the area of the WH throat does not deviate considerably from the horizon area of the extremal RN BH (again at $\mu = 0$).

For gauged solutions, the behaviour is qualitatively very similar. We show this in Fig. 7, that corresponds to models with $q/\mu = 0.2$. The main difference occurs close to the limit configurations (the red curve), for which the mass take relatively large negative values, as compared with the ungauged case. On the other hand, for sufficiently large values of the fermion mass, the throat area is slightly smaller than the horizon area of the extremal RN BH.

Figures 6 and 7 indicate that, for a fixed value of the fermion mass, there is a minimum charge below which it is not possible to form a smooth symmetric WH. For this minimum charge, the mass is also minimal, while the value of the throat area is always of the order of magnitude of the extremal RN BH with the corresponding electric charge.

The results also indicate that it is possible to have WH solutions with arbitrarily large mass and charge, and relatively small values of the fermion mass. The geometry of such WHs do not differ much from the geometry of extremal RN, with the main differences occurring only close to the throat.

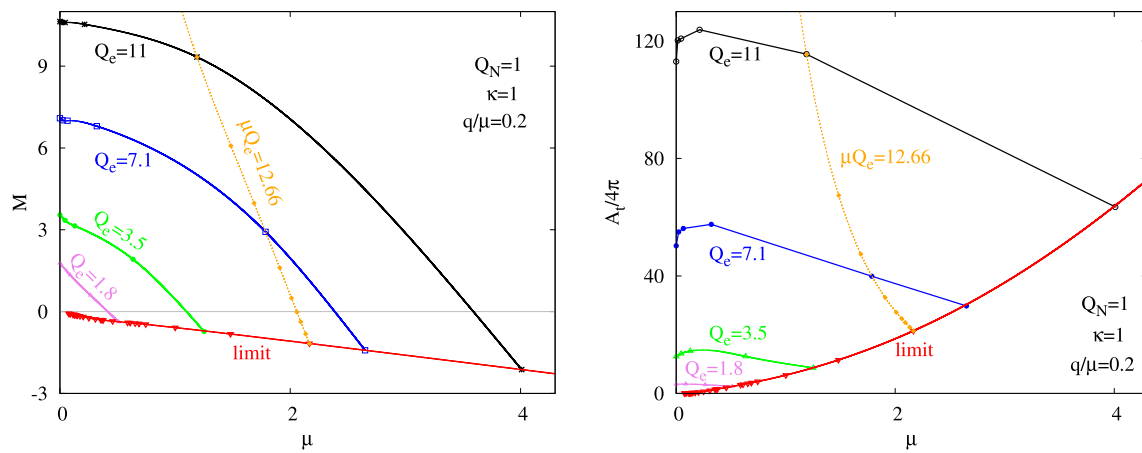


Fig. 7 (left) Mass M vs μ in Plank units for solutions with $q/\mu = 0.2$. The color curves correspond to families of solutions with fixed electric charge ($Q_e = 1.8, 3.5, 7.1, 11$ in pink, green, blue and black respectively). In red we show the limit configurations with $w_* = -\mu$. In

orange we include the solutions with fixed $\mu Q_e = 12.66$ for comparison with Fig. 4(right). Same figure for the throat area A_t as a function of μ

5 Further remarks

The main purpose of this work was to provide a detailed description of the construction and of the (basic) properties of a new type of WH solutions reported in Ref. [21]. As with their Finster–Smoller–Yau solitonic counterparts [10,18], these Einstein–Dirac–Maxwell (EDM) configurations are spherically symmetric, with two massive fermions in a singlet spinor state. Also, they are free of singularities, representing localized states, with a finite mass M and electric charge Q_e .

One should remark that the existence of two asymptotic regions for a WH geometry introduces a number of complications in the formulation of a consistent ansatz, as compared to the solitonic case. The main difficulties can be traced back to the fact that, different from the case of bosonic fields, a Dirac field necessarily implies a tetrad choice, with the existence of some special features at the WH throat [34]. Another complication originates in choosing to study WH geometries which are symmetric with respect to a reflection at the throat.

Interestingly, all symmetric solutions are overcharged, their systematic analysis revealing that the extremal Reissner–Nordström (RN) BHs play an important role, as providing one of the boundaries of the domain of existence, for which the mass/charge ratio is maximal. The other boundary of the domain of existence is given by a set of limit configurations, for which the mass/charge ratio is minimal. We have shown that, in principle, one can obtain WH solutions with bulk geometries very similar to extremal RN, only significantly different close to the throat, which is supported by the fermionic matter. On the other hand, we find that the throat area of the WHs we have considered do not differ significantly

cantly with respect the horizon area of a extremal RN BH of the same charge.

Let us close this Section with a discussion of possible issues and open questions on the subject of WHs in EDM theory. First, a better understanding of the behaviour at the WH’s throat of the metric and matter functions is clearly necessary. For example, as mentioned in Sect. 3, the first derivative of the radial metric function is discontinuous at the WH throat, for all solutions in this work. However, this is likely a consequence of the assumption of reflection symmetry, and one expect this feature to be absent for *asymmetric* WH geometries.

In our construction, these wormholes are supported by Dirac and Maxwell fields, a matter content that lays within the standard model of physics. No ‘exotic’ matter, in the sense of hypothetical fields, such as phantom fields or complex scalars, are necessary for the construction of these wormholes. However, we have also shown that, because of the spinor fields, the null energy condition is violated everywhere. Although a hypothesis, there are reasonable arguments to expect that ‘regular’ matter should indeed satisfy some form of the energy conditions [39], in particular when considering quantum effects. It would be interesting to analyze what is the effect of introducing quantum effects in the wormholes we have discussed, but such endeavor is beyond the scope of this paper.

On the other hand, it is well known that WHs generically possess dynamical instabilities, already at the level of spherically symmetric perturbations [40–44]. Therefore it is possible that the EDM WH also possess similar instabilities.

Finally, the most challenging issue is to understand the physical relevance of this type of solutions. As with the Finster–Smoller–Yau solitons [10,18], the construction

here employs a semiclassical approach. That is, the Dirac–Maxwell and Einstein equations are coupled, the fermionic nature of the Dirac field being imposed at the level of the occupation number, only. The debate on the physical validity of this approach has a long history (see e.g. the discussion between Wheeler and de Witt in Ref. [45], p. 143). While a final answer here is absent in the literature, one expects that the inclusion of quantum corrections to the Dirac stress–energy tensor [46,47] may affect the properties of the solutions or even invalidate them (if they are on the same order of magnitude (or larger) as those found within the *quantum wave function* approach). However, there are also arguments that the employed treatment (without a second quantization of the Dirac field) may provide a reasonable approximation under certain conditions, see e.g. Refs. [48,49]. Moreover, we expect EDM WHs to exist as well in a more complete setting, with a fully quantized (gauged) Dirac field, as suggested by the results in [50].

Acknowledgements We would like to thank D. Danielson, G. Satishchandran, R. Wald and R. Weinbaum for insightful remarks on a first version of this draft. The work of E. R. is supported by the Fundacao para a Ciéncia e a Tecnologia (FCT) project UID/MAT/04106/2019 (CIDMA) and by national funds (OE), through FCT, I.P., in the scope of the framework contract foreseen in the numbers 4, 5 and 6 of the article 23, of the Decree-Law 57/2016, of August 29, changed by Law 57/2017, of July 19. We acknowledge support from the project PTDC/FIS-OUT/28407/2017 and PTDC/FIS-AST/3041/2020. This work has further been supported by the European Union’s Horizon 2020 research and innovation (RISE) programmes H2020-MSCA-RISE-2015 Grant No. StronGrHEP-690904 and H2020-MSCA-RISE-2017 Grant No. FunFiCO-777740. The authors would like to acknowledge networking support by the COST Actions CA15117 CANTATA and CA16104 GWverse. JLBS gratefully acknowledges support by the DFG Research Training Group 1620 *Models of Gravity* and the DFG project BL 1553.

Data Availability Statement This manuscript has no associated data or the data will not be deposited. [Authors’ comment: The data presented in this study are available on request from the corresponding author.]

Open Access This article is licensed under a Creative Commons Attribution 4.0 International License, which permits use, sharing, adaptation, distribution and reproduction in any medium or format, as long as you give appropriate credit to the original author(s) and the source, provide a link to the Creative Commons licence, and indicate if changes were made. The images or other third party material in this article are included in the article’s Creative Commons licence, unless indicated otherwise in a credit line to the material. If material is not included in the article’s Creative Commons licence and your intended use is not permitted by statutory regulation or exceeds the permitted use, you will need to obtain permission directly from the copyright holder. To view a copy of this licence, visit <http://creativecommons.org/licenses/by/4.0/>. Funded by SCOAP³.

A Dirac field: the general formalism

In what follows we shall use the conventions and notation used in Ref. [33]. Coordinate indices are denoted with Greek

letters $\alpha, \beta, \gamma \dots$ and tetrad basis indices with Roman letters a, b, c, \dots . Also, ∂_μ, ∇_μ and \hat{D}_μ are used to denote partial, covariant and spinor derivatives, respectively.

One starts by defining a set of four tetrads $e_a = e_a^\alpha \frac{\partial}{\partial x^\alpha}$, with

$$e_a^\alpha = \{e_0^\alpha, e_1^\alpha, e_2^\alpha, e_3^\alpha\}, \quad (\text{A.1})$$

which we take to be an orthonormal basis, *i.e.*,

$$g_{\alpha\beta} e_a^\alpha e_b^\beta = \eta_{ab}, \quad \text{with } \eta_{ab} = \text{diag}(-1, 1, 1, 1). \quad (\text{A.2})$$

Also

$$e_\alpha^a = \eta^{ab} g_{\alpha\beta} e_b^\beta \quad \text{and} \quad g_{\alpha\beta} = \eta_{ab} e_\alpha^a e_\beta^b. \quad (\text{A.3})$$

To define the gamma matrices, we start by introducing two sets of 4×4 matrices γ^α and $\hat{\gamma}^a$ which satisfy the relation (where $\{A, B\} = AB + BA$):

$$\{\gamma^\alpha, \gamma^\beta\} = 2g^{\alpha\beta} I_4, \quad \{\hat{\gamma}^a, \hat{\gamma}^b\} = 2\eta^{ab} I_4, \quad (\text{A.4})$$

with

$$\gamma^\alpha = e_a^\alpha \hat{\gamma}^a, \quad \text{and} \quad \hat{\gamma}_a = \eta_{ab} \hat{\gamma}^b, \quad \gamma_\alpha = g_{\alpha\beta} \gamma^\beta. \quad (\text{A.5})$$

Our choice for the matrices $\tilde{\gamma}$ is

$$\tilde{\gamma}^0 = \begin{pmatrix} O & I \\ I & O \end{pmatrix}, \quad \tilde{\gamma}^i = \begin{pmatrix} O & \sigma_i \\ -\sigma_i & O \end{pmatrix}, \quad i = 1, 2, 3, \quad (\text{A.6})$$

where σ_i are the Pauli matrices

$$\sigma_1 = \begin{pmatrix} 0 & 1 \\ 1 & 0 \end{pmatrix}, \quad \sigma_2 = \begin{pmatrix} 0 & -i \\ i & 0 \end{pmatrix}, \quad \sigma_3 = \begin{pmatrix} 1 & 0 \\ 0 & -1 \end{pmatrix}, \quad (\text{A.7})$$

I is the 2×2 identity and O is the 2×2 zero matrix.

The matrices $\hat{\gamma}^a$ are defined as

$$\hat{\gamma}^1 = i\tilde{\gamma}^3, \quad \hat{\gamma}^2 = i\tilde{\gamma}^1, \quad \hat{\gamma}^3 = i\tilde{\gamma}^2, \quad \hat{\gamma}^0 = i\tilde{\gamma}^0. \quad (\text{A.8})$$

Furthermore, we also define the Dirac conjugate

$$\bar{\Psi} \equiv \Psi^\dagger \alpha, \quad (\text{A.9})$$

where $\alpha = -\hat{\gamma}^0$ and Ψ^\dagger the Hermitian conjugate of Ψ . Also, the spinor covariant derivative \hat{D}_ν is defined as

$$\hat{D}_\nu = \partial_\nu - \Gamma_\nu, \quad (\text{A.10})$$

while the covariant derivative of the conjugate spinor is

$$\hat{D}_\mu \bar{\Psi} = \partial_\mu \bar{\Psi} + \bar{\Psi} \Gamma_\mu. \quad (\text{A.11})$$

The spinor connection matrices Γ_ν is defined in terms of the spin-connection $w_{\mu ab}$ [33]

$$\Gamma_\alpha = -\frac{1}{4} w_{\alpha bc} \hat{\gamma}^b \hat{\gamma}^c, \quad \text{with } w_{\mu_b}^a = e_\nu^a e_b^\lambda \Gamma_{\mu\lambda}^\nu - e_b^\lambda \partial_\mu e_\lambda^a, \quad (\text{A.12})$$

$\Gamma_{\mu\lambda}^\nu$ being the Christoffel symbols associated with $g_{\alpha\beta}$.

B Dirac equation on a spherically symmetric background: separability

The Dirac operator on the spherically symmetric background (3.1) takes the form

$$\gamma^\nu \hat{D}_\nu = \frac{\epsilon_t}{F_0} \hat{\gamma}^t (\partial_t - iqV) + \frac{\epsilon_r}{F_1} \hat{\gamma}^r \left[\partial_r + \partial_r (\ln F_2 \sqrt{F_0}) \right] + \frac{i}{F_2} \hat{\gamma}^r \hat{\gamma}^t \mathcal{K}, \tag{B.1}$$

with the operator

$$\mathcal{K} = i \hat{\gamma}^t \hat{\gamma}^r \left[\hat{\gamma}^\theta \left(\partial_\theta + \frac{\cos \theta}{\sin \theta} \right) + \frac{1}{\sin \theta} \hat{\gamma}^\phi \partial_\phi \right] \tag{B.2}$$

being the angular Dirac operator (the Dirac operator on the two sphere [51]). By construction we have $[\mathcal{D}, \mathcal{K}] = 0$ and $[\mathcal{D}, \partial_t] = 0$.

The Dirac equation (B.1) is decoupled when considering the Ansatz (3.7), since

$$\mathcal{K} \Psi^{[1,2]} = \pm \kappa \Psi^{[1,2]} \tag{B.3}$$

$$\partial_t \Psi^{[1,2]} = -i\omega \Psi^{[1,2]} \tag{B.4}$$

Choosing the parametrization (3.8), after some algebraic manipulations, the Dirac equation (B.1) can be reduced to the differential equations (3.11). We further constrain to spinors with $|\kappa| = 1$. Then, by choosing the radial dependence of the spinor $\Psi^{[1,2]}$ as in Eq. (3.8) further simplifies the total stress energy momentum tensor, becoming diagonal and compatible with a spherically symmetric line element [16, 18, 52].

C Details on the numerical approach

In the numerics, we have found convenient to define a new radial (compactified) coordinate ρ ,

$$\rho = \text{sign}(r) \sqrt{1 - \frac{r_0}{\sqrt{r^2 + r_0^2}}} \tag{C.1}$$

such that $\rho \rightarrow \pm 1$ as $r \rightarrow \pm\infty$, while $\rho = 0$ for $r = 0$.

Then the line element (3.1) takes the following form, as written in terms of ρ together with a redefinition of the metric functions, $F_0 = \sqrt{\sigma}$ and $F_1 = 1/\sqrt{n}$:

$$ds^2 = -\sigma(\rho) dt^2 + \frac{4r_0^2}{(1-\rho^2)^2} \frac{d\rho^2}{n(\rho)} + \frac{r_0^2}{(1-\rho^2)^2} d\Omega^2. \tag{C.2}$$

Also, in numerics we employ two new spinor functions f, g , with

$$P = \frac{1}{\sqrt{2}}(f - g), \quad Q = \frac{1}{\sqrt{2}}(f + g). \tag{C.3}$$

With the above redefinitions, the Einstein–Dirac–Maxwell Eqs. (3.10), (3.11) (3.12) take the following form

$$\frac{d\sigma}{d\rho} = -\frac{1-\rho^2}{2\rho} \left(\frac{dV}{d\rho} \right)^2 + \frac{16\epsilon_r r_0 \sigma}{\sqrt{n}\rho(1-\rho^2)} \left(g \frac{df}{d\rho} - f \frac{dg}{d\rho} \right) + \frac{2\sigma(1-n\rho^2)}{n\rho(1-\rho^2)}, \tag{C.4}$$

$$\frac{dn}{d\rho} = \frac{2}{\rho} \frac{1-n}{1-\rho^2} - \frac{n}{\sigma} \frac{1-\rho^2}{2\rho} \left(\frac{dV}{d\rho} \right)^2 - \frac{32r_0^2 \epsilon_t (w+qV)}{\sqrt{\sigma}\rho(1-\rho^2)^3} (f^2 + g^2), \tag{C.5}$$

$$\frac{df}{d\rho} = -\frac{1+3\rho^2 n}{2n\rho(1-\rho^2)} f - \frac{2\epsilon_r \kappa}{\sqrt{n}(1-\rho^2)} f - \frac{2\epsilon_r r_0 \mu}{\sqrt{n}(1-\rho^2)^2} g + \frac{2r_0 \epsilon_r \epsilon_t (w+qV)}{\sqrt{n}\sigma(1-\rho^2)^2} g + \frac{1-\rho^2}{8\sigma\rho} \left(\frac{dV}{d\rho} \right)^2 f + \frac{8r_0^2 \mu}{n\rho(1-\rho^2)^3} (g^2 - f^2) f + \frac{16\kappa r_0}{n\rho(1-\rho^2)^2} f^2 g - \frac{8r_0^2 \epsilon_t (w+qV)}{\sqrt{\sigma}n\rho(1-\rho^2)^3} (f^2 + g^2) f, \tag{C.6}$$

$$\frac{dg}{d\rho} = -\frac{1+3\rho^2 n}{2n\rho(1-\rho^2)} g + \frac{2\epsilon_r \kappa}{\sqrt{n}(1-\rho^2)} g - \frac{2\epsilon_r r_0 \mu}{\sqrt{n}(1-\rho^2)^2} f - \frac{2r_0 \epsilon_r \epsilon_t (w+qV)}{\sqrt{n}\sigma(1-\rho^2)^2} f + \frac{1-\rho^2}{8\rho\sigma} \left(\frac{dV}{d\rho} \right)^2 g + \frac{8r_0^2 \mu}{n\rho(1-\rho^2)^3} (g^2 - f^2) g + \frac{16\kappa r_0}{n\rho(1-\rho^2)^2} g^2 f - \frac{8r_0^2 \epsilon_t (w+qV)}{\sqrt{\sigma}n\rho(1-\rho^2)^3} (f^2 + g^2) g, \tag{C.7}$$

$$\frac{d^2 V}{d\rho^2} = \frac{32\epsilon_t q r_0^2 \sqrt{\sigma}}{n(1-\rho^2)^4} (f^2 + g^2) + \left[\frac{1}{\rho} - \frac{32r_0 \kappa}{n\rho(1-\rho^2)^2} f g + \frac{16r_0^2 \mu}{n\rho(1-\rho^2)^3} (f^2 - g^2) + \frac{32r_0^2 \epsilon_t (w+qV)}{\sqrt{\sigma}n\rho(1-\rho^2)^3} (f^2 + g^2) \right] \frac{dV}{d\rho}, \tag{C.8}$$

which was used in the numerics. Let us remark that the Einstein Eqs. (3.10) contain also an extra second order equation.

This equation was treated as a constraint, being used to monitor the accuracy of the numerical results.

The above system of five non-linear coupled differential equations for the functions n , σ and f , g , V was solved by using the software package COLSYS [53].

This solver employs a collocation method for boundary-value ordinary differential equations and a damped Newton method of quasi-linearization. Typical meshes use around 10^4 points in the interval $-1 \leq \rho \leq 1$. At each iteration step a linearized problem is solved by using a spline collocation at Gaussian points. The typical relative accuracy for the solutions reported here was around 10^{-10} .

In order to solve numerically the previous system of equations, one has to provide numerical values of a number of input parameters. To specify a theory, one should fix the value of μ and q (fermion mass and charge respectively). The vielbein ansatz must be fixed by choosing the signs ϵ_t and ϵ_r . The spinor depends on the parameters κ and w , while the throat size is fixed with the value of r_0 . Other parameters are imposed as boundary conditions. For instance, the total electric charge is fixed by requiring $\frac{dV}{d\rho}(1) = \frac{2Q_e}{r_0}$, and we focus on solutions with $f(0) = 0$. In practice, once a seed solution is obtained, we explore the space of solutions by keeping all parameters fixed except r_0 and w . Deforming the seed solution by changing these two parameters allows us to obtain the WH configurations with $\frac{d\sigma}{d\rho}(0) = 0$, which are the ones reported in this work.

D An exact solution

As remarked in Ref. [21], the $q = w = \mu = 0$ limit of the Einstein–Dirac–Maxwell equations allows for a simple exact WH solution, which captures some basic properties of the more general solutions discussed above. The expression of this solution has been given in⁴ [21] in Schwarzschild-like coordinates, with $F_2 = r$. For the choice (3.2) of the metric-gauge, the functions which enter the line element (3.1) are

$$\begin{aligned} F_0(r) &= 1 - \frac{2Q_e^2 r_0}{Q_e^2 + r_0^2} \frac{1}{F_2(r)}, \\ F_1(r) &= \frac{\sqrt{1 + \frac{r_0}{F_2(r)}}}{\sqrt{1 - \frac{Q_e^2}{r_0 F_2(r)}}}, \quad F_2(r) = \sqrt{r^2 + r_0^2}, \end{aligned} \quad (\text{D.1})$$

with the matter functions

$$\begin{aligned} P(r) &= U_1(r) - U_2(r), \quad Q(r) = U_1(r) + U_2(r), \\ V(r) &= \pm \frac{2Q_e r_0}{Q_e^2 + r_0^2} \end{aligned}$$

⁴ The same line element has been obtain in Ref. [54,55] as a possible metric in a brane world supported by a bulk-induced tidal stress–energy tensor.

$$\sqrt{\left(1 - \frac{Q_e^2}{r_0 F_2(r)}\right) \left(1 - \frac{r_0}{F_2(r)}\right)}, \quad (\text{D.2})$$

where

$$\begin{aligned} U_1(r) &= \frac{c_0}{\sqrt{F_0(r)}} \left(\sqrt{1 - \frac{Q_e^2}{r_0 F_2(r)}} - \kappa \sqrt{1 - \frac{r_0}{F_2(r)}} \right)^2, \\ U_2(r) &= \frac{\kappa r_0}{32c_0(Q_e^2 + r_0^2)\sqrt{F_0(r)}} \\ &\quad \left(\sqrt{1 - \frac{Q_e^2}{r_0 F_2(r)}} + \kappa \sqrt{1 - \frac{r_0}{F_2(r)}} \right)^2. \end{aligned} \quad (\text{D.3})$$

This solution contains three essential parameters (r_0 , Q_e) and c_0 (with $r_0 > Q_e$), its mass being

$$M = \frac{2Q_e^2 r_0}{Q_e^2 + r_0^2}, \quad (\text{D.4})$$

(note that $Q_e/M > 1$). One can easily see that the metric and the spinor functions do not change under the transformation $r \rightarrow -r$, containing even functions of r only, while for $V(r)$ one can take $V(-r) = -V(r)$ without any loss of generality (note that $V(0) = 0$, while $\Phi = \pm M/Q_e$). Also, the first derivatives of the metric functions F_i vanish at $r = 0$, and thus there is no thin mass shell structure at the throat.

This WH geometry is supported by the spinors contribution to the total energy-momentum tensor, being regular everywhere (for example, the Ricci scalar vanishes, while the Kretschmann scalar is finite and smooth everywhere). Also, as $Q_e \rightarrow r_0$, the extremal Reissner–Nordström BH is approached, the Dirac stress energy tensor vanishing.

However, this solution possesses some undesirable features. In particular, the spinor functions (P , Q) do not vanish as $r \rightarrow \pm\infty$. Therefore, the spinor wave function is not normalizable, and one cannot impose the one particle condition, $Q_N = 1$.

References

1. D. Ivanenko, Sov. Phys. **13**, 141 (1938)
2. H. Weyl, Phys. Rev. **77**, 699 (1950)
3. W. Heisenberg, Physica **19**, 897 (1953)
4. R. Finkelstein, R. LeLevier, M. Ruderman, Phys. Rev. **83**, 326 (1951)
5. R. Finkelstein, C.F. Fronsdal, P. Kaus, Phys. Rev. **103**, 1571 (1956)
6. M. Soler, Phys. Rev. D **1**, 2766 (1970)
7. T. Cazenave, L. Vazquez, Commun. Math. Phys. **105**, 35–47 (1986)
8. S.R. Coleman, Nucl. Phys. B **262**, 263 (1985) (**Erratum: Nucl. Phys. B 269 (1986), 744**)
9. C.A.R. Herdeiro, E. Radu, Symmetry **12**(12), 2032 (2020). [arXiv:2012.03595](https://arxiv.org/abs/2012.03595) [gr-qc]
10. F. Finster, J. Smoller, S.T. Yau, Phys. Rev. D **59**, 104020 (1999). [arXiv:gr-qc/9801079](https://arxiv.org/abs/gr-qc/9801079)
11. D.R. Brill, J.A. Wheeler, Rev. Mod. Phys. **29**, 465–479 (1957)
12. T.D. Lee, Y. Pang, Phys. Rev. D **35**, 3678 (1987)

13. D.J. Kaup, Klein–Gordon geon. *Phys. Rev.* **172**, 1331 (1968)
14. R. Ruffini, S. Bonazzola, Systems of self-gravitating particles in general relativity and the concept of an equation of state. *Phys. Rev.* **187**, 1767 (1969)
15. I. Pena, D. Sudarsky, *Class. Quantum Gravity* **14**, 3131 (1997)
16. F. Finster, J. Smoller, S.T. Yau, *Commun. Math. Phys.* **205**, 249–262 (1999). [arXiv:gr-qc/9810048](#)
17. F. Finster, J.A. Smoller, S.T. Yau, [arXiv:gr-qc/9910030](#)
18. F. Finster, J. Smoller, S.T. Yau, *Phys. Lett. A* **259**, 431–436 (1999). [arXiv:gr-qc/9802012](#)
19. F. Finster, J. Smoller, S.T. Yau, *Nucl. Phys. B* **584**, 387–414 (2000). [arXiv:gr-qc/0001067](#)
20. C. Herdeiro, I. Perapechka, E. Radu, Y. Shnir, *Phys. Lett. B* **797**, 134845 (2019). [arXiv:1906.05386](#) [gr-qc]
21. J.L. Blázquez-Salcedo, C. Knoll, E. Radu, *Phys. Rev. Lett.* **126**(10), 101102 (2021). [arXiv:2010.07317](#) [gr-qc]
22. J.A. Wheeler, *Geometrodynamics* (Academic, New York, 1962)
23. H.G. Ellis, *J. Math. Phys.* **14**, 104–118 (1973)
24. K.A. Bronnikov, *Acta Phys. Pol. B* **4**, 251–266 (1973)
25. M.S. Morris, K.S. Thorne, *Am. J. Phys.* **56**, 395–412 (1988)
26. M. Visser, *Lorentzian Wormholes: from Einstein to Hawking* (American Institute of Physics, Woodbury, 1995)
27. F.S.N. Lobo, *Int. J. Mod. Phys. D* **25**(07), 1630017 (2016). [arXiv:1604.02082](#) [gr-qc]
28. T. Kodama, *Phys. Rev. D* **18**, 3529 (1978)
29. C. Armendariz-Picon, *Phys. Rev. D* **65**, 104010 (2002)
30. H. Huang, J. Yang, *Phys. Rev. D* **100**, 124063 (2019)
31. P. Kanti, B. Kleihaus, J. Kunz, *Phys. Rev. Lett.* **107**, 271101 (2011). [arXiv:1108.3003](#) [gr-qc]
32. C. Barcelo, M. Visser, *Class. Quantum Gravity* **17**, 3843–3864 (2000). [arXiv:gr-qc/0003025](#)
33. S.R. Dolan, D. Dempsey, *Class. Quantum Gravity* **32**(18), 184001 (2015). [arXiv:1504.03190](#) [gr-qc]
34. M. Cariglia, G.W. Gibbons, [arXiv:1806.05047](#) [gr-qc]
35. D.L. Danielson, G. Satishchandran, R.M. Wald, R.J. Weinbaum, *Phys. Rev. D* **104**(12), 124055 (2021). <https://doi.org/10.1103/PhysRevD.104.124055>. [arXiv:2108.13361](#) [gr-qc]
36. R.A. Konoplya, A. Zhidenko, [arXiv:2106.05034](#) [gr-qc]
37. K. Bronnikov, S. Bolokhov, S. Krasnikov, M. Skvortsova, [arXiv:2104.10933](#) [gr-qc]
38. C.A.R. Herdeiro, A.M. Pombo, E. Radu, *Phys. Lett. B* **773**, 654–662 (2017). [arXiv:1708.05674](#) [gr-qc]
39. E.A. Kontou, K. Sanders, *Class. Quantum Gravity* **37**(19), 193001 (2020). <https://doi.org/10.1088/1361-6382/ab8fcf>. [arXiv:2003.01815](#) [gr-qc]
40. H.A. Shinkai, S.A. Hayward, *Phys. Rev. D* **66**, 044005 (2002). [arXiv:gr-qc/0205041](#)
41. J.A. Gonzalez, F.S. Guzman, O. Sarbach, *Class. Quantum Gravity* **26**, 015010 (2009). [arXiv:0806.0608](#) [gr-qc]
42. J.A. Gonzalez, F.S. Guzman, O. Sarbach, *Class. Quantum Gravity* **26**, 015011 (2009). [arXiv:0806.1370](#) [gr-qc]
43. F. Cremona, F. Pirota, L. Pizzocchero, *Gen. Relativ. Gravit.* **51**(1), 19 (2019). [arXiv:1805.02602](#) [gr-qc]
44. J.L. Blázquez-Salcedo, X.Y. Chew, J. Kunz, *Phys. Rev. D* **98**(4), 044035 (2018). [arXiv:1806.03282](#) [gr-qc]
45. The Role of Gravitation in Physics, Report from the 1957 Chapel Hill Conference, Cécile M. DeWitt and Dean Rickles (eds.), Edition Open Access (2011)
46. L.E. Parker, D. Toms, *Quantum Field Theory in Curved Spacetime* (Cambridge University Press, Cambridge, 2009)
47. P.B. Groves, P.R. Anderson, E.D. Carlson, *Phys. Rev. D* **66**, 124017 (2002)
48. C. Armendariz-Picon, P.B. Greene, *Gen. Relativ. Gravit.* **35**, 1637–1658 (2003). [arXiv:hep-th/0301129](#)
49. F. Finster, J. Smoller, S.T. Yau, *Mod. Phys. Lett. A* **14**, 1053–1057 (1999). [arXiv:gr-qc/9906032](#)
50. J. Maldacena, A. Milekhin, F. Popov, [arXiv:1807.04726](#) [hep-th]
51. A.A. Abrikosov, Jr., Dirac operator on the Riemann sphere. [arXiv:hep-th/0212134](#)
52. J.L. Blázquez-Salcedo, C. Knoll, *Eur. Phys. J. C* **80**(2), 174 (2020). [arXiv:1910.03565](#) [gr-qc]
53. U. Ascher, J. Christiansen, R.D. Russell, *Math. Comput.* **33**(146), 659–679 (1979)
54. K.A. Bronnikov, S.W. Kim, *Phys. Rev. D* **67**, 064027 (2003). [arXiv:gr-qc/0212112](#)
55. K.A. Bronnikov, V.N. Melnikov, H. Dehnen, *Phys. Rev. D* **68**, 024025 (2003). [arXiv:gr-qc/0304068](#)